ORNL/TM-2023/3194

DYNAMIC BEAM SHAPE SENSING AND CONTROL IN AN OPEN ARCHITECTURE METAL AM SYSTEM FOR MICROSTRUCTURE MANIPULATION

CRADA Final Report - NFE-19-07880

Gerry Knapp
Alex Plotkowski
Peter Wang

October 2023

OAK RIDGE National Laboratory

ORNL IS MANAGED BY UT-BATTELLE LLC FOR THE US DEPARTMENT OF ENERGY

ORNL/TM-2023/3194

Division or Program Name

DYNAMIC BEAM SHAPE SENSING AND CONTROL IN AN OPEN ARCHITECTURE METAL AM SYSTEM FOR MICROSTRUCTURE MANIPULATION

Gerry Knapp, Alex Plotkowski, Peter Wang

October 2023

Prepared by
OAK RIDGE NATIONAL LABORATORY
Oak Ridge, TN 37831
managed by
UT-BATTELLE LLC
for the
US DEPARTMENT OF ENERGY
under contract DE-AC05-00OR22725

CONTENTS

ABSTRACT

Most commercially available metal additive manufacturing (AM) systems are closed-architecture, meaning that the system manufacturer limits the ability of the user to directly control the process conditions and can modify the specified inputs using proprietary methods. Unfortunately, this approach severely limits or confounds the ability for users to perform research on fundamental aspects of additive manufacturing. ARCTOS Technology Solutions (ARCTOS) produces an open-architecture laser powder bed fusion (PBF) additive manufacturing system that allows the user to fully control all aspects of the process control and monitoring. The purpose of this project is to help develop beam shaping capabilities and controls within the ARCTOS open-architecture system for control of microstructure evolution during metal AM.

1. BACKGROUND

The localized control of microstructure during additive manufacturing processing is an opportunity for obtaining an improvement in component performance, both structural and functional. Within the last several years, the MDF has shown significant advances in controlling the microstructure of Ni-base superalloys using electron beam additive manufacturing [1–6]. Electron beam melting has been the primary focus for microstructure control due to the flexibility of the software architecture for manipulating the system and the possibility of complex scan strategies enabled by the rapid motion of the beam. However, electron beam AM is not suitable for all materials, and can be limited by process expense, surface roughness, and materials selection. Conversely, most laser powder bed systems have closed software architectures that restrict scan pattern design and can dynamically modify the laser parameters, such as laser power, based on proprietary algorithms developed by the manufacturers. There are also physical limitations due to the laser galvanometer hardware that controls laser motion, which does not allow for the same flexibility of scan pattern control to the same extent as electron beams.

Open-architecture laser control software and hardware that increases the design space for laser scan paths would expand the ability Having access to the laser control software architecture allows for certainty that the specified parameters were executed by the system. Additionally, recent research in tuning laser optics [7–9] is a promising path for control of the melt pool behavior in laser systems, creating opportunities for control of microstructure and properties based on dynamic control of the heat source power distribution. Additional control of the heat source motion combined with beam shaping capabilities offers a significant design space for improved control of microstructure and defect formation during laser powder bed additive manufacturing.

The purpose of this project is for MDF and ARCTOS Technology Solutions, LLC (ARCTOS, formerly the Universal Technology Corporation) to collaborate on the control and process monitoring of scan pattern and dynamic beam shaping within an open architecture selective laser melting system. Successful use of such a system will require a fundamental understanding of materials science in relevant alloy systems, use of modeling tools for determining the influence of beam shape on solidification characteristics, and sensing and data analytics capabilities for *in situ* process monitoring and control.

2. RESEARCH APPROACH AND METHODS

One of the emerging materials in PBF processing is aluminum alloys, which can have exceptional mechanical and high-temperature properties due to the rapid solidification experienced during additive manufacturing [10]. For this reason, the effect of laser processing parameters on the microstructure of aluminum alloys was investigated. Two approaches were taken to the research. First, a beam shaping

optical lens was installed in the optics chain. This static beam shaping optic was intended to change the shape of the beam from a circular beam cross-section to an elliptical beam cross-section. The effective beam shape during laser process is sometimes modified through optics or rapid laser oscillation to produce melt pools that are less susceptible to hot-cracking during welding and with varying microstructure [11-13]. Secondly, control of the scan path from the open-source architecture was used to have direct control over the processing parameters.

The Direct Machine Control (DMC) software provided with the open architecture system was used to design and control the laser scan path for a process parameter design matrix. To investigate the effect of scan parameters on the melt pool and microstructure, square regions of bi-directional raster scans were done on plates of cast A356 ingot. Aluminum plate had to be used as a surrogate for aluminum powder due to safety regulations surrounding aluminum powder storage and processing in the ORNL Manufacturing Demonstration Facility. In each square region, the laser power, scan speed, and hatch spacing were specified parametrically using the values specified in Table 1. The size of the squares was 150 mm x 150 mm and they were spaced with 50 mm between each square in a row. Figure 1 shows the layout of the samples in rows and columns on the two A356 substrates. The full process parameter list corresponding with each of these pads is provided in Appendix A Table A1.

Table 1. Process parameters for area melts on A356 substrate

Process parameter (unit)	**Nominal value**		**Variables values**		
Laser power (W)	250		150, 200, 250, 300, 350		
Laser scan speed (m/s)	1.0		0.5, 0.75, 1.0, 1.25, 1.5		
Hatch overlap, predicted (%,)	60		10, 20, 40, 60, 70		
Constant Linear Energy Cases (250 J/m)					
Laser power (W)	150	200	250	187.5	312.5
Laser scan speed (m/s)	0.6	0.8	1.0	0.75	1.25

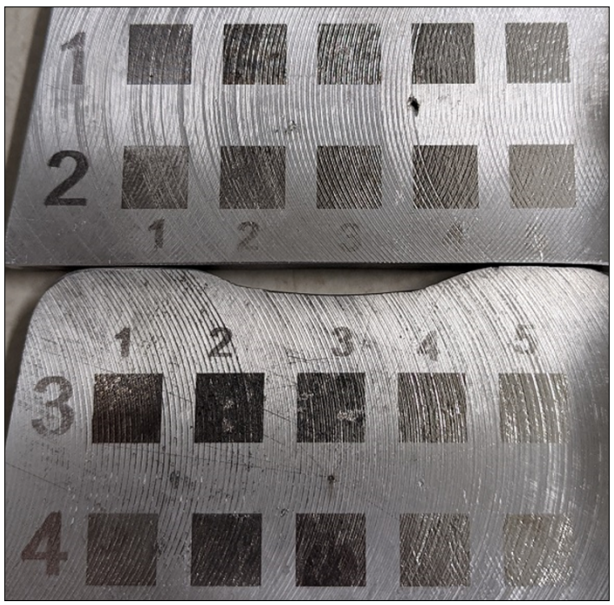

Figure 1. Process parameter test matrix on machined A356 samples.

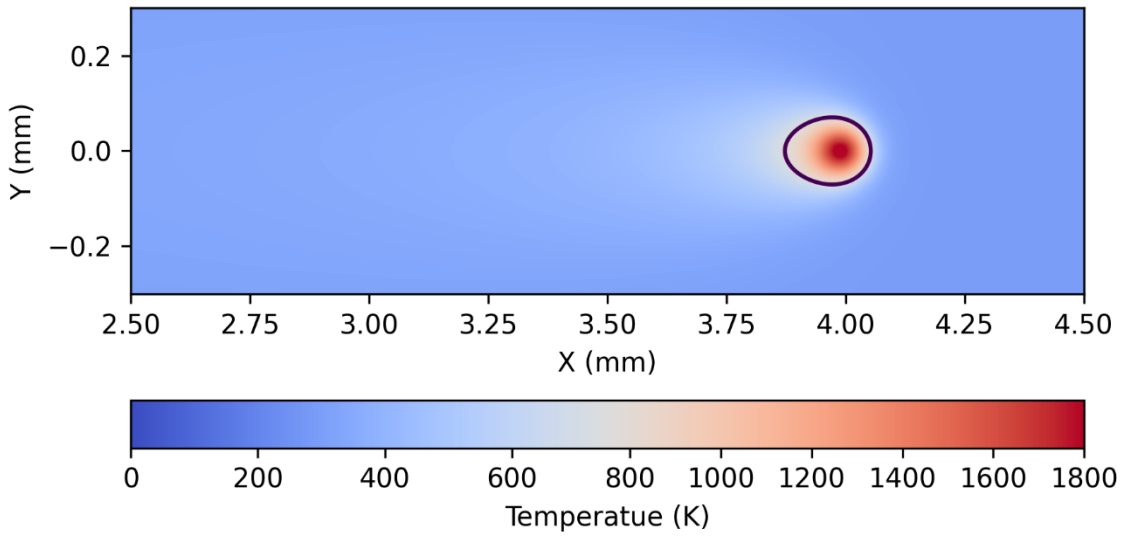

Figure 2. Use of 3DThesis [14] to estimate hatch spacing to achieve different hatch spacing overlaps.

The samples were sectioned perpendicular to the scan direction and mounted in epoxy. A grinding and polishing procedure for aluminum was applied to the mounted samples, ending in a final polishing step using 1 micron diamond polishing abrasive on a nap cloth. The polished samples were then imaged using optical microscopy, which contrasts the aluminum matrix and eutectic Al-Si phase that form in the solidification microstructure of aluminum A356.

3. RESULTS AND DISCUSSION

During installation of the ARCTOS system at the ORNL MDF, the beam shaping optics were installed and the beam geometry was measured using a beam profilometer. These measurements showed no significant differences in the beam shape with and without the beam shaping optics. The data on the beam shaping was not properly recorded, so the data cannot be reproduced here. The beam shaping optics were removed from the system before the effects of process parameter variations were investigated.

The process parameters used to produce the surface-melted squares melted the surface in all cases, as observed by the change in the surface finish of the A356 plate shown in Figure 1. The samples were sectioned and mounted to enable microscopy of the transverse cross-section of the melted regions, i.e., the cross-section perpendicular to the raster direction of the scan pattern. The resulting optical micrographs are presented in Figure 3. Despite every sample melting, the sectioned samples revealed that the depth of melting in some cases was very shallow. Figure 4 shows the depth of the melted region as a function of the linear energy input into the system (laser power divided by the scan velocity). As the power input into the system was increased, the depth expectedly increased. In the cases with lower linear energy, the depth was only 10-20 microns, which would likely be too shallow for process in a layer-by-layer processing with actual powder. For the range of process parameters tested here, relatively high energy input is needed to overcome the high reflectivity and high thermal diffusivity of aluminum alloys.

Besides the variations in melt pool depths, another major variation was observed in the degree of liquid mixing. The degree of liquid metal mixing can be inferred from the extent that the substrate dendrite structure can still be seen in the final melt pool. In the cases with fast scanning speeds, such as the 1.5 m/s scan speed case and the 312 W & 1.25 m/s case, the original dendrite structure can still be clearly seen in

the melted region. In cases with slower scan speeds, such as the 187W & 0.75 m/s case, the Al dendrite and Al-Si interdendritic region can be seen to be mixed more homogeneously. In actual PBF conditions, the region where melted material interacts with the substrate will likely be removed when cutting the part from the build plate, so this is not of great concern. However, aluminum is a low melting point alloy that is susceptible to selective vaporization of alloying elements during laser processing [15], so increased fluid flow in the melt pool may be desirable to more evenly distribute heat input from the laser and reduce the amount of vaporization.

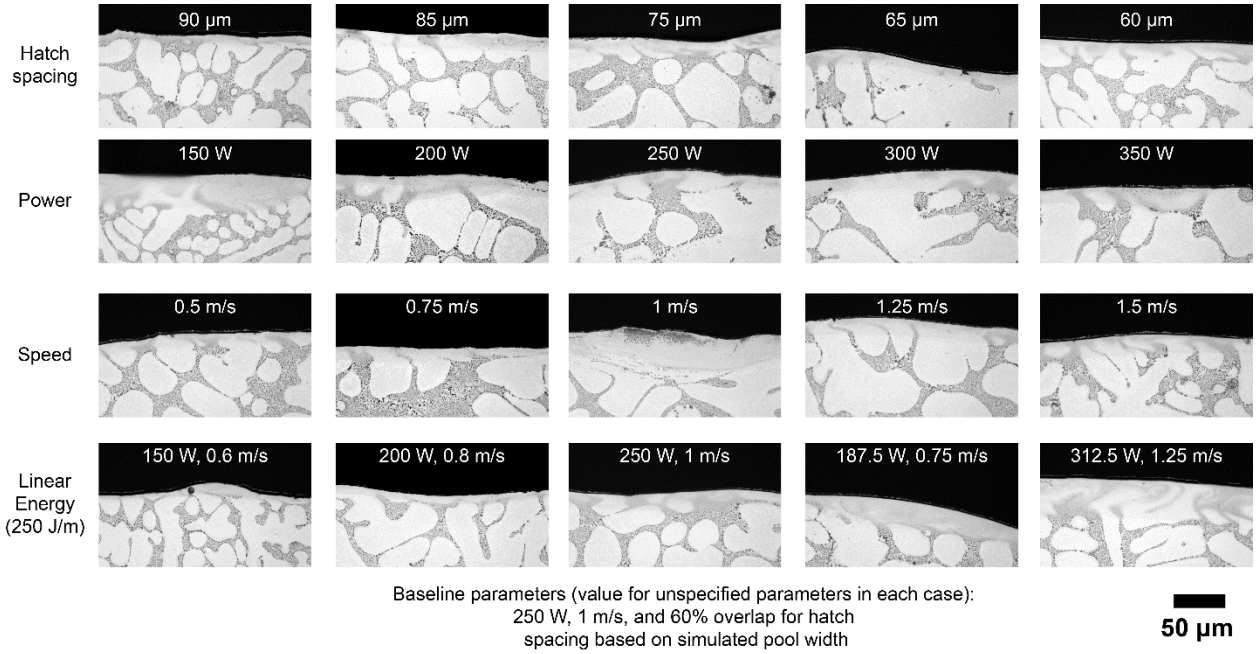

Figure 3. Optical micrographs of the microstructure in the cast substrate and melted regions for a range of process parameters.

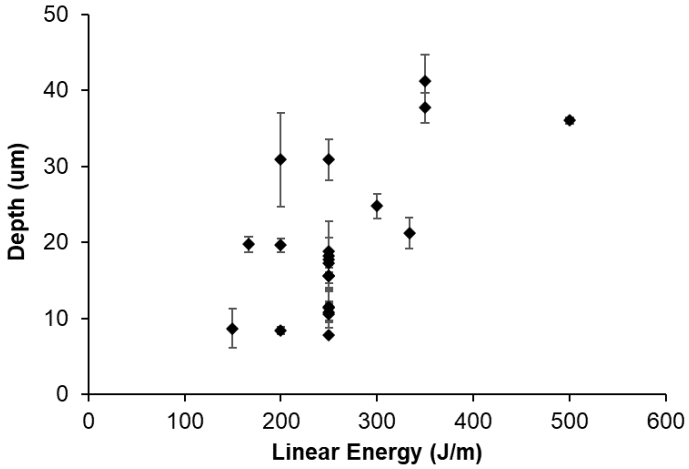

Figure 4. Change in melt pool depth as a function of linear energy. Error bars show the standard deviation of three measurements for the melted depth at different locations in the sample.

The main consequence of incomplete mixing was the lack of ability to determine the interdendritic spacing for every melt pool. An example of how to measure the interdendritic spacing for one of the more thoroughly-mixed microstructures is shown in Figure 5. The red line in Figure 5(a) shows a region with sufficient contrast between the Al dendrites and the Al-Si interdendritic region. The corresponding grayscale signal is shown in Figure 5(b). The distance between the peaks (Al-rich regions) can be interpreted as an estimate the dendrite spacing. When the mixing in the melt pool was poor, there was low contrast between the dendrites and interdendritic regions generated by the laser remelting. Therefore, a detailed analysis of the microstructure scale for all process conditions could not be conducted. However, it is clear that the dendritic scale of the microstructure in the melted regions is significantly reduced compared to the as-cast material. The melted region has dendrites on the scale of a couple of microns, whereas the as-cast microstructure has dendrites that are 10-100 microns wide.

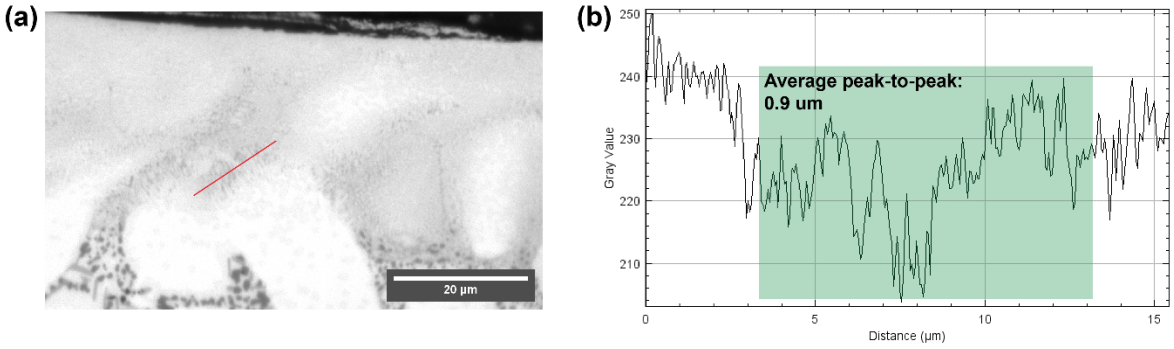

Figure 5. (a) Micrograph of the laser surface melt with 150W laser power, 0.6 m/s scan speed, 40 micron hatch spacing. A red line indicates the location of a line intensity plot. The lighter phase is the Al matrix and the darker phase is the Si eutectic phase (b) Line intensity plot of the grayscale value. The green highlighted region shows the region used for peak-to-peak analysis to approximate the dendrite spacing of the laser melted material.

4. CONCLUSIONS

In this work, the open-source controller for the ARCTOS powder bed system was used to generate characteristic single-layer melting of a cast aluminum alloy. This enabled for a straightforward generation of a design of experiments. While the beam shaping optics were not effective in changing the beam shape, obvious changes in the melt pool geometry and microstructure features were observed. Notably, the melt pool size and degree of melt pool mixing changed significantly as a function of the laser power and scanning speed. In order to achieve reasonable processing parameters, lower scanning speeds with variable laser power produced reasonably deep melt pools with a good degree of mixing in the melt pool. Ultimately, there are still opportunities to pursue dynamic beam shaping possibilities for powder bed fusion. Based on the results seen here, dynamic changes in the process parameters during PBF processing would lead to different melt pool characteristics.

5. REFERENCES

[1] R.R. Dehoff, M.M. Kirka, W.J. Sames, H. Bilheux, A.S. Tremsin, L.E. Lowe, S.S. Babu, Site specific control of crystallographic grain orientation through electron beam additive manufacturing, Mater. Sci. Technol. 31 (2015) 931–938. doi:10.1179/1743284714Y.0000000734.

[2] M.M. Kirka, Y. Lee, D.A. Greeley, A. Okello, M.J. Goin, M.T. Pearce, R.R. Dehoff, Strategy for Texture Management in Metals Additive Manufacturing, JOM. 69 (2017) 523–531. doi:10.1007/s11837-017-2297-7.

[3] N. Raghavan, R. Dehoff, S. Pannala, S. Simunovic, M. Kirka, J. Turner, N. Carlson, S.S. Babu, Numerical modeling of heat-transfer and the influence of process parameters on tailoring the grain morphology of IN718 in electron beam additive manufacturing, Acta Mater. 112 (2016) 303–314. doi:10.1016/j.actamat.2016.03.063.

[4] N. Raghavan, S. Simunovic, R. Dehoff, A. Plotkowski, J. Turner, M. Kirka, S. Babu, Localized melt-scan strategy for site specific control of grain size and primary dendrite arm spacing in electron beam additive manufacturing, Acta Mater. 140 (2017). doi:10.1016/j.actamat.2017.08.038.

[5] A. Plotkowski, M.M. Kirka, S.S. Babu, Verification and Validation of a Rapid Heat Transfer Calculation Methodology for Transient Melt Pool Solidification Conditions in Powder Bed Metal Additive Manufacturing, Addit. Manuf. 18 (2017) 256–268. doi:10.1016/j.addma.2017.10.017.

[6] J. Raplee, A. Plotkowski, M.M. Kirka, R.B. Dinwiddie, A. Okello, R.R. Dehoff, S.S. Babu, Thermographic Microstructure Monitoring in Electron Beam Additive Manufacturing, Nat. Sci. Reports. (2017) 1–16. doi:10.1038/srep27398.

[7] T.T. Roehling, S.S.Q. Wu, S.A. Khairallah, J.D. Roehling, S. Stefan Soezeri, M.F. Crumb, M.J. Matthews, Modulating laser intensity profile ellipticity for microstructural control during metal additive manufacturing, Acta Mater. 128 (2017) 197–206. doi:10.1016/j.actamat.2017.02.025.

[8] M.A. Vorontsov, Additive Manufacturing in Metals with a Fiber Array laser Source and Adaptive Multi-Beam Shaping, 15/642884, 2019.

[9] M.A. Vorontsov, Additive Manufacturing in Metals with a Fiber Array laser Source and Adaptive Multi-Beam Shaping, 15/983866, 2019.

[10] A. Shyam, A. Plotkowski, S. Bahl, K. Sisco, L.F. Allard, Y. Yang, J.A. Haynes, R.R. Dehoff, An additively manufactured AlCuMnZr alloy microstructure and tensile mechanical properties, Mater. 12 (2020) 100758. DOI: doi:10.1016/j.mtla.2020.100758.

[11] L. Wang, M. Gao, C. Zhang, X. Zeng, Effect of beam oscillating pattern on weld characterization of laser welding of AA6061-T6 aluminum alloy, Materials & Design 108 (2016) 707-717. DOI: https://doi.org/10.1016/j.matdes.2016.07.053.

[12] L. Wang, M. Gao, X. Zeng, Experiment and prediction of weld morphology for laser oscillating welding of AA6061 aluminium alloy, Science and Technology of Welding and Joining 24(4) (2019) 334-341. DOI: 10.1080/13621718.2018.1551853.

[13] W. Li, Y. Xia, Y. Fang, H. Song, J. Lei, Effects of circular beam oscillation on microstructure, mechanical and electrochemical corrosion properties of laser melting deposited Inconel 625, Journal of Manufacturing Processes 84 (2022) 847-858. DOI: https://doi.org/10.1016/j.jmapro.2022.10.059.

[14] B. Stump, 3DThesis, 2021. https://gitlab.com/JamieStumpORNL/3DThesis.

[15] A. Klassen, V.E. Forster, C. Körner, A multi-component evaporation model for beam melting processes, Modelling and Simulation in Materials Science and Engineering 25(2) (2017) 025003.

APPENDIX A. FULL PARAMETER STUDY CASES

The table below provides all values relevant to the process parameters for the parameter study experiment. This expands the data provided in Table 1. Each section of the table shows the series of experiments that intentionally varied a single process parameter with other values held constant. The varied process parameter is highlighted in yellow for each section.

Table A1. Full parameter set with melt pool width predictions.

Row	Col.	Power (W)	Speed (m/s)	Linear Energy (J/m)	Hatch Spacing (µm)	Overlap (%)	Estimated melt pool width (µm)
1	1	250	1	250	90	10	102
1	2	250	1	250	85	20	102
1	3	250	1	250	75	40	102
1	4	250	1	250	65	60	102
1	5	250	1	250	60	70	102
		Power (W)					
2	1	150	1	150	30	60	48
2	2	200	1	200	50	60	82
2	3	250	1	250	65	60	102
2	4	300	1	300	75	60	118
2	5	350	1	350	80	60	130
			Speed (m/s)				
3	1	250	0.5	500	75	60	120
3	2	250	0.75	333	70	60	110
3	3	250	1	250	65	60	102
3	4	250	1.25	200	60	60	96
3	5	250	1.5	166	55	60	92
				Linear Energy (J/m)			
4	1	150	0.6	250	40	60	62
4	2	200	0.8	250	55	60	88
4	3	250	1	250	65	60	102
4	4	187.5	0.75	250	50	60	82
4	5	312.5	1.25	250	70	60	114